Send Orders for Reprints to reprints@benthamscience.ae

Open Access

Analysis of a Kinematic Model for a Forestry Six-Wheeled Luffing Articulated Vehicle Chassis

Han Dongtao[1,2], Liu Jinhao[*,1], Kan Jiangming[1] and Tang Weiguo[1]

[1]*Beijing Forestry University, Beijing 100083, China*

[2]*Hulunbuir College, Inner Mongolia Automomous Region 021000, China*

Abstract: The chassis is a key component of forestry vehicular equipment that directly determines its ability to drive and climb in rough mountainous or forested terrain. A six-wheeled luffing articulated chassis was designed to scale obstacles on forested land. This paper discusses the use of the Devanit-Hartenberg method to establish a kinematic model for this vehicle chassis; positive solutions of the kinematic model were then applied to an analysis of the luffing capabilities of the six-wheeled luffing articulated chassis. Theoretical calculations, simulations, and experimental results showed that the established kinematic model can be applied to the development and production of forestry equipment.

Keywords: D-H kinematic model, luffing ability, six-wheeled luffing articulated chassis.

1. INTRODUCTION

Woodland and forest conditions can be difficult for vehicles and various mobile devices (*e.g.*, robots) to navigate. At present, despite the many engineered chassis available, it is difficult to find one that provides good climbing performance with strong adaptability for overcoming the many small obstacles encountered on rough roads in highly dense forested areas.

Common mobile robots can be divided into wheeled mobile robots, legged mobile robots, and tracked robots. The wheel-legged mobile mechanism improves the robot's climbing ability, particularly over obstacles. Four types of wheel-legged robots have been described in recent studies. Based on the geometric constraint angle, Xin *et al*. investigated the obstacle-surmounting ability of track-legged robots [1]. Iagnemma *et al*. analyzed the climbing ability of a six-wheeled rocker-arm robot, based on a quasi-steady state model [2]. Lamon and Krebs established a mechanical model of the climbing dynamics of wheel-legged robots [3]. Hu *et al*. studied the obstacle-crossing problem of a lunar rover [4]. In all of these studies, luffing played a key role in the ability of the robot to overcome the obstacle in its path.

The wheel-legged luffing chassis structure is a typical chassis structure, with the advantages of flexible adjustment in attitude for a given terrain, flexible obstacle avoidance, and obstacle crossing/climbing capabilities. This multifunctional chassis allows for various modes of movement, including walking, turning left and right, crossing convex platforms, climbing stairs, and crossing trenches and barriers [5].

*Address correspondence to this author at the Beijing Forestry University, Beijing 100083, China; Tel: 010-62336204; Fax: 010-62336204;
E-mail: liujinhao@vip.163.com

In this study, we describe a luffing articulated chassis with automatic attitude adjustment, which was designed and applied to forestry vehicles capable of handling forest conditions in China. The six-wheeled frame improves the ground adaptability of the mobile chassis and provides enhanced stability for transport applications. The wheel legs of the six-wheeled luffing articulated chassis can also be adjusted to the topographic characteristics of a region, which improves the obstacle-surmounting capability of the vehicle. Additionally, the coordinated movement of the four separate wheel-legged structures effectively improves the overstepping ability and terrain adaptability of the chassis. To verify the work performance of the designed six-wheeled luffing articulated chassis under woodland road conditions, a kinematic model was created based on Denavit-Hartenberg (D-H) methodology [6-11]. This kinematic model was used to analyze the transformation capacity of the front and rear legs and the movement characteristics of the chassis. Based on the results of the analysis, the kinematic model was revised and optimized. Good agreement was obtained between simulation results with the optimized model and measurement results. Thus, our results demonstrate that this model can provide a basis for further studies of movement characteristics for chassis design.

2. KINEMATICS MODEL BUILDING

2.1. Introduction of Structures

In the design of the six-wheeled luffing articulated chassis, we took into consideration the climbing and articulated steering ability of the vehicle, as well as its adaptability to forest terrain. Fig. (**1**) shows the six-wheeled luffing articulated chassis and a virtual prototype. The right-front leg of the chassis is controlled by electric putters 1 and 2 (Fig. **1**); the same configuration is used for the left-front leg. Electric putter 4 controls the right rear leg, as well as the

1874-155X/15 2015 Bentham Open

left rear leg. Two articulated steering electric putters control the retractable steering. The right-front leg (coordinate 8 in Fig. **1**) is connected to the rear frame though the rear leg body hinge point, and the articulated structure of the "V"-shaped wheel leg (coordinate 13, Fig. **1**) facilitates climbing.

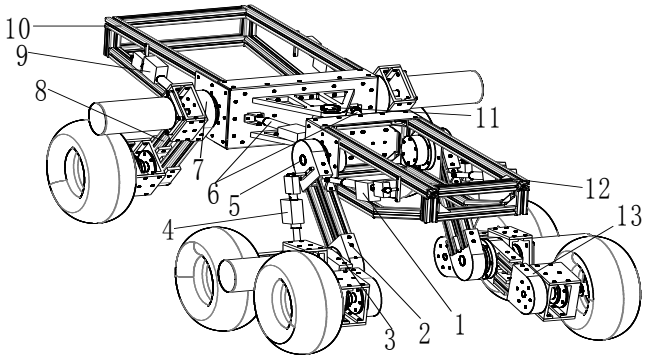

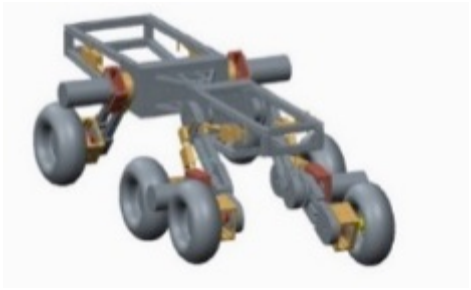

Fig. (1). Six-wheeled luffing articulated chassis and virtual prototype: 1. electric putter 1; 2. right-front wheel leg; 3. hinge point of the "V"-shaped structure; 4. electric putter 2; 5. chassis body hinge point of the right-front wheel legs; 6. articulated steering electric putter 3; 7. chassis body hinge point of right rear wheel legs; 8. right rear wheel legs; 9. electric putter 4; 10. rear frame; 11. articulated steering hinge point; 12. front frame; and 13. "V"-shaped wheel leg.

2.2. Chassis Coordinate System Based on the D-H Method

The six-wheeled luffing articulated chassis, as a vehicle travel mechanism, consists of four separate wheeled legs that work cooperatively to complete the command function. The chassis coordinate system [6, 12, 13], shown in Fig. (**2**), is described below. The positive *x*-axis direction is defined as the forward direction. The right-front wheeled-leg coordinate systems are, in order, defined as Nos. 1, 3, and 5 (with 5 corresponding to the wheel center). The left-front wheeled-leg coordinate systems are, in order, Nos. 2, 4, and 6 (the wheel center is 6). The right-rear wheeled-leg coordinate systems are, in order, Nos. 9, 10, and 12 (the wheel center is 12). The left-rear wheeled-leg coordinate systems are, in order, Nos. 9, 11, and 13 (the wheel center is 13). The articulated steering joint coordinate system corresponds to No. 9. Fig. (**2**) shows the relationship among the coordinates, which is based on the D-H method; the D-H parameters for the wheel center coordinates (5, 6, 12, and 13) are listed in Table **1**.

The vertical dimensions between hinge points 1 and 2 and coordinate O (a_1 and a_2, respectively) are $a_1 = a_2 =$ 238 mm and between hinge points 10 and 11 and coordinate O (a_3 and a_4, respectively) are $a_3 = a_4 =$ 316 mm. The length of the front legs is $L_1 = L_2 =$ 467 mm. The length of the front "V"-shaped legs is $L_3 = L_4 =$ 301 mm. The length of the rear legs is $L_{10} = L_{11} =$ 439 mm. The distance in the *x*-axis direction from hinge point 9 to the front part of the front frame is $P_1 =$ 732 mm, and that to the back end of the rear frame is $P_2 =$ 297 mm. The angle of the right-front wheeled-leg hinge point 1, with respect to the *x*-axis, is θ_1.

Table 1. Devanit-Hartenberg (D-H) parameters.

Frame		θ	D	a	α
Right front leg	1	0	a_1	0	0
	3	θ_1	0	L_1	0
	5	θ_3	0	L_3	0
Left front leg	2	0	$-a_2$	0	0
	4	θ_2	0	L_2	0
	6	θ_4	0	L_4	0
Right rear leg	9	180	0	P_1	−90
	10	θ_{10}	0	$\sqrt{a_3^2 + p_2^2}$	−90
	12	180-θ_{12}	0	L_{10}	0
Left rear leg	9	180	0	P_1	−90
	11	θ_{11}	0	$\sqrt{a_4^2 + p_2^2}$	−90
	13	180-θ_{13}	0	L_{11}	0

The angle of the "V"-shaped leg hinge point 3, with respect to the *x*-axis, is θ_3. Similarly, the angles of the left-front wheeled leg with respect to the *x*-axis are θ_2 and θ_4. The articulated steering angles of the right-rear wheeled leg and left-rear leg about the *y*-axis are θ_{10} and θ_{11}, respectively. The angles of the rear wheeled legs 8 and 9 about the *z*-axis are θ_{12} and θ_{13}, respectively, as shown in Fig. (**2**).

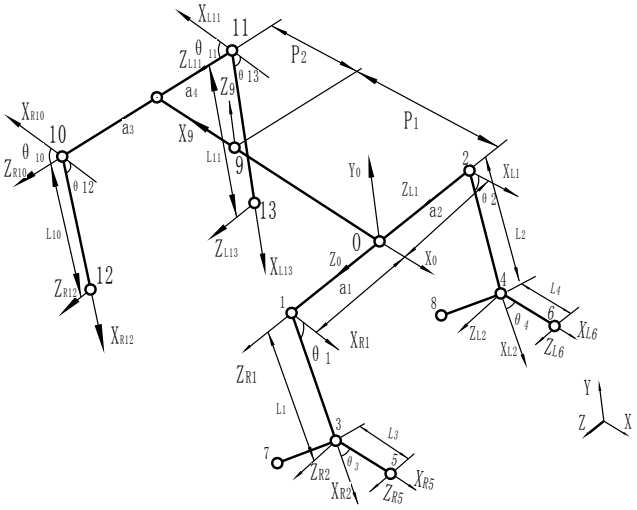

Fig. (2). Coordinate system of the six-wheeled luffing articulated chassis.

3. DERIVATION OF THE KINEMATIC MODEL

The D-H method is a useful tool for space geometry kinematics. It is mainly based on the assumption that the robot is composed of a series of joints and connecting rods. Connecting rods can rotate around the joints, which can be placed in any order and in any plane. The length of a connecting rod is arbitrary (*i.e.*, any value is possible, including zero) and can be bent or distorted for any plane. Any set of joints and connecting rods constitutes a robot model. A reference coordinate system is set at each joint. Transformations are performed to connect one joint to the next, up to the last joint. A series of transformation steps provides the total transformation for the robotic vehicle's motion.

3.1. Kinematic Model Based on the D-H Method

Coordinates $(0, X_0, Y_0, Z_0)$ are shown in Fig. (**2**). Based on the D-H method, if ${}^0T_1$ describes the position and attitude of the first connecting rod relative to the reference coordinate system, then ${}^1T_2$ describes the position and attitude of the second connecting rod relative to first connecting rod. The position and attitude of the second connecting rod in the reference coordinates is given by the following matrix product:

$$A_2 = {}^0T_1 {}^1T_2$$

In a similar way, A_3 describes the position and attitude of the third connecting rod to the second connecting rod, with $A_3 = {}^0T_3 = {}^0T_1 {}^1T_2 {}^2T_3$.

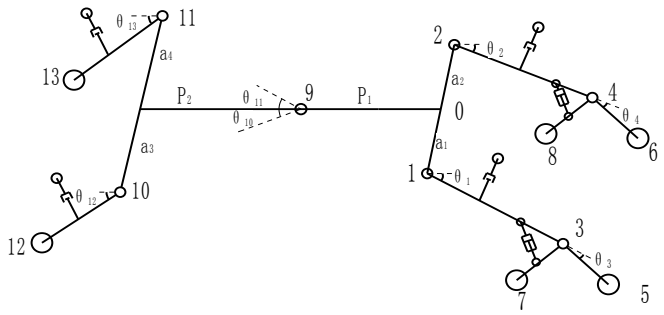

Fig. (3). Structure diagram for the six-wheeled luffing articulated chassis.

3.2. Six-Wheeled Luffing Articulated Chassis Transform Matrix

As an example, we use the right-front wheeled leg and right-rear wheeled leg to characterize the luffing motion. Fig. (**3**) shows the structure diagram for this example. Here, the left-front wheeled-leg structure (coordinates: 2, 4, 6, and 8) and the right-front wheeled-leg structure (coordinates: 1, 3, 5, and 7) have the same movement characteristics, as does the left-rear wheeled leg (coordinates: 9, 11, and 13) and the right-rear wheeled leg (coordinates: 9, 10, and 12).

In the D-H method, the right-front wheeled leg (coordinates: 1, 3, 5, and 7) is defined as follows:

$${}^{i-1}T_i = \begin{bmatrix} c\theta_i & -s\theta_i & 0 & a_{i-1} \\ s\theta_i c\alpha_{i-1} & c\theta_i c\alpha_{i-1} & -s\alpha_{i-1} & -d_i s\alpha_{i-1} \\ s\theta_i s\alpha_{i-1} & c\theta_i s\alpha_{i-1} & c\alpha_{i-1} & d_i c\alpha_{i-1} \\ 0 & 0 & 0 & 1 \end{bmatrix}$$

$$T_i = \begin{bmatrix} c\theta_i & -s\theta_i c\alpha_i & s\theta_i s\alpha_i & a_i c\theta_i \\ s\theta_i & c\theta_i c\alpha_i & -c\theta_i s\alpha_i & a_i s\theta_i \\ 0 & s\alpha_i & c\alpha_i & d_i \\ 0 & 0 & 0 & 1 \end{bmatrix}$$

The relationship between the forward reference coordinate system and the right-front wheeled-leg coordinate system (coordinates: 1, 3, 5, and 7), as shown in Figs. (**2**, **3**) and Table **1**, can be calculated using the D-H method. The general form of each connecting rod's transformation matrix can be simplified as follows:

$${}^0T_1 = \begin{bmatrix} 1 & 0 & 0 & 0 \\ 0 & 1 & 0 & 0 \\ 0 & 0 & 1 & a_1 \\ 0 & 0 & 0 & 1 \end{bmatrix} \qquad {}^1T_3 = \begin{bmatrix} c_1 & s_1 & 0 & L_1 c_1 \\ -s_1 & c_1 & 0 & -L_1 s_1 \\ 0 & 0 & 1 & 0 \\ 0 & 0 & 0 & 1 \end{bmatrix}$$

$${}^3T_5 = \begin{bmatrix} c_3 & -s_3 & 0 & L_3 C_3 \\ S_3 & C_3 & 0 & L_3 S_3 \\ 0 & 0 & 1 & 0 \\ 0 & 0 & 0 & 1 \end{bmatrix}$$

The coordinate conversion of wheel center 5 (Figs. **2**, **3**), relative to the reference coordinates, is given by $A_5 = {}^0T_5 = {}^0T_1\,{}^1T_3\,{}^3T_5$, as shown below:

$$\begin{bmatrix} 1 & 0 & 0 & 0 \\ 0 & 1 & 0 & 0 \\ 0 & 0 & 1 & a_1 \\ 0 & 0 & 0 & 1 \end{bmatrix} \begin{bmatrix} c_1 & s_1 & 0 & L_1c_1 \\ -s_1 & c_1 & 0 & -L_1s_1 \\ 0 & 0 & 1 & 0 \\ 0 & 0 & 0 & 1 \end{bmatrix}$$

$$\begin{bmatrix} c_3 & -s_3 & 0 & L_3C_3 \\ S_3 & C_3 & 0 & L_3S_3 \\ 0 & 0 & 1 & 0 \\ 0 & 0 & 0 & 1 \end{bmatrix} = \begin{bmatrix} n_x & o_x & a_x & p_x \\ n_y & o_y & a_y & p_y \\ n_z & o_z & a_z & p_z \\ 0 & 0 & 0 & 1 \end{bmatrix}.$$

The coordinate of the right-front wheel center (coordinate 5, Figs. **2**, **3**) in the reference coordinate system is as follows:

$$P_x = L_3\cos(\theta_1 - \theta_3) + L_1\cos\theta_1 \tag{1}$$

$$p_y = -\left[L_3\sin(\theta_1 - \theta_3) + L_1\sin\theta_1\right] \tag{2}$$

$$p_z = a_1 \tag{3}$$

Similarly, the coordinate of the left-front wheel center (coordinate 6, Figs. **2**, **3**) in the reference coordinate system is

$$P_x = L_4\cos(\theta_2 - \theta_4) + L_2\cos\theta_2 \tag{4}$$

$$p_y = -\left[L_4\sin(\theta_2 - \theta_4) + L_2\sin\theta_2\right] \tag{5}$$

$$p_z = a_1 \tag{6}$$

3.3. Pose Transform of the Right Rear Wheel Center with Positive Kinematics

${}^0T_9$ represents the matrix converted from the basic coordinate (0, X_0, Y_0, Z_0) to coordinate 9; ${}^9T_{10}$ is the converted matrix from coordinate 9 to coordinate 10; and ${}^{10}T_{12}$ is the converted matrix from coordinate 10 to coordinate 12, as given below:

$${}^0T_9 = \begin{bmatrix} -1 & 0 & 0 & -p_1 \\ 0 & 0 & -1 & 0 \\ 0 & -1 & 0 & 0 \\ 0 & 0 & 0 & 1 \end{bmatrix}$$

$${}^9T_{10} = \begin{bmatrix} c_{10} & 0 & -s_{10} & \sqrt{a_3^2 + p_2^2}\,c_{10} \\ s_{10} & 0 & c_{10} & \sqrt{a_3^2 + p_2^2}\,s_{10} \\ 0 & -1 & 0 & 0 \\ 0 & 0 & 0 & 1 \end{bmatrix}$$

$${}^{10}T_{12} = \begin{bmatrix} -c_{12} & -s_{12} & 0 & -L_{10}c_{12} \\ s_{12} & -c_{12} & 0 & L_{10}s_{12} \\ 0 & 0 & 1 & 0 \\ 0 & 0 & 0 & 1 \end{bmatrix}$$

$${}^0T_{12} = \begin{bmatrix} c_{10}c_{12} & c_{10}s_{12} & s_{10} & L_{10}c_{10}c_{12} - \sqrt{a_3^2 + p_2^2}\,c_{10} - p_1 \\ s_{12} & -c_{12} & 0 & L_{10}s_{12} \\ c_{12}s_{10} & s_{10}s_{12} & -c_{10} & L_{10}c_{12}s_{10} - \sqrt{a_3^2 + p_2^2}\,s_{10} \\ 0 & 0 & 0 & 1 \end{bmatrix} = \begin{bmatrix} n_x & o_x & a_x & p_x \\ n_y & o_y & a_y & p_y \\ n_z & o_z & a_z & p_z \\ 0 & 0 & 0 & 1 \end{bmatrix}$$

The coordinates of the right-rear wheel center (coordinate 12, Figs. **2**, **3**) in the reference coordinate system are

$$P_x = L_{10}c_{10}c_{12} - \sqrt{a_3^2 + p_2^2}\,c_{10} - p_1 \tag{7}$$

$$p_y = L_{10}s_{12} \tag{8}$$

$$p_z = L_{10}c_{12}s_{10} - \sqrt{a_3^2 + p_2^2}\,s_{10} \tag{9}$$

The coordinates of the left-rear wheel center (coordinate 13, Figs. **2**, **3**) in the reference coordinate system are

$$P_x = L_{11}c_{11}c_{13} - \sqrt{a_4^2 + p_2^2}\,c_{11} - p_1 \tag{10}$$

$$p_y = L_{11}s_{13} \tag{11}$$

$$p_z = L_{11}c_{13}s_{11} - \sqrt{a_4^2 + p_2^2}\,s_{11} \tag{12}$$

3.4. Theory Analysis of the Right-Front Wheeled-Leg Kinematics Model in the Luffing Process

Luffing analysis for the *y*-axis was carried out on the right-front wheel leg. Based on the luffing motion, the displacement variation regulation of the "V"-shaped wheeled leg center (coordinate 5, Figs. **2**, **3**), relative to the 0 point along the *y*-axis of the reference coordinate system, is given as follows:

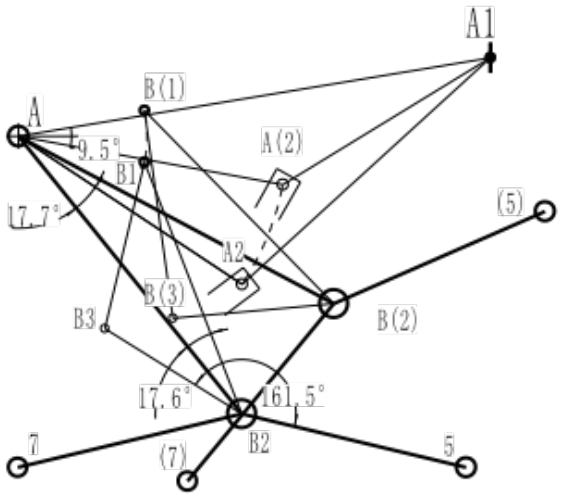

Fig. (4). Schematic diagram of right-front wheeled leg luffing.

Fig. (**4**) shows the position relationship of each hinge point of the front wheeled-leg electric putters 1 and 2 (A_1A_2 and B_1B_3 in Fig. **4**). The installation angles of hinge points A_1 and A_2 are 9.5° and 17.7°, respectively. The installation angles of hinge points B_3 and B_1 are 161.5° and 17.6°, respectively. The corresponding transformation is as follows:

$$\theta_1=\angle A_1AA_2+17.7^\circ-9.5^\circ \quad (13)$$

$$\theta_3=180^\circ-161.5^\circ-17.6^\circ+\angle A_1AA_{(2)} \quad (14)$$

As shown in Fig. (**4**), hinge joint A_2 between the front wheeled-leg of electric putter 1 and wheeled leg 2, hinge joint A_1 of the front frame 12 （in Fig. **1**), and hinge joint A of front wheeled leg 2 and front frame 12 make up the triangle $\triangle AA_1A_2$, with $AA_1=625$ mm AA_2=351 mm; $A_1A_{2\max}=440$ mm ; $A_1A_{2\min}=320$ mm, $\cos\angle A_1AA_2$ =0.73, and $\angle A_1AA_2=43.1^\circ$, when the initial displacement of electric putter 1 is at a maximum, namely, $A_1A_{2\max}=440$ mm.

After the transformation:

$\theta_{1\max}=\angle A_1AA_2+17.7^\circ-9.5^\circ=51.3^\circ$.

Similarly, $\cos\angle A_1AA_{(2)}=0.94$, and $\angle A_1AA_{(2)}=20.3^\circ$ when the final displacement of electric putter 1 is at its minimum value, namely, $A_1A_{2\min}=320$ mm.

After the transformation:

$\theta_{1\min}=\angle A_1AA_{(2)}+17.7^\circ-9.5^\circ=28.5^\circ$

Thus, θ_1 changes from 51.3° to 28.5° when the displacement of electric putter 1 changes from a maximum of 440 mm to a minimum of 320 mm.

Similarly, for electric putter 2, wheeled leg 2 and "V"-shaped leg 13 make up triangle $\triangle B_1B_2B_3$, with $B_1B_2=354$ mm, $B_1B_{3\max}=275$ mm, $B_1B_{3\min}=225$ mm, and $B_2B_3=211$ mm. The corresponding angle for B_2B_3 is $\angle B_1B_2B_3$.

When the initial displacement of electric putter 2 is at a minimum,

$\cos\angle B_1B_2B_3=0.8$, $\angle B_1B_2B_3=36.9^\circ$, and

$\theta_{3\min}=180^\circ-161.5^\circ-17.6^\circ+\angle B_1B_2B_3=37.8^\circ$.

When the final displacement of electric putter 2 is at a maximum,

$\cos\angle B_{(1)}B_{(2)}B_{(3)}=0.63$, $\angle B_{(1)}B_{(2)}B_{(3)}=50.9^\circ$, and

$\theta_{3\max}=180^\circ-161.5^\circ-17.6^\circ+\angle B_{(1)}B_{(2)}B_{(3)}=51.8^\circ$.

The corresponding angle changes from 37.8° to 51.8° when electric putter 2 changes from a minimum displacement of 225 mm to a maximum displacement of 275 mm, as shown in Fig. (**4**). For the front wheel-legged mechanism, the right-front wheeled leg can reach a maximum in the *y* direction when θ_1 reaches its minimum value ($\theta_{1\min}$) and θ_3 reaches its maximum value ($\theta_{3\max}$), namely, $\theta_1=28.5^\circ$ and $\theta_3=51.8^\circ$, respectively.

According to Eq. (2):

$p_{y\text{front}}$= -434.8*mm* (initial displacement relative to reference coordinate) and $p_{y\text{front max}}$= -104*mm* (final displacement relative to the reference coordinate). The maximum range in the *y* direction is $|p_{y\text{front}Y}|$ = |-434.8-(-104)| = 330.8 mm.

To verify the luffing rule, we set θ_3 to be constant, namely, $\theta_3=37.8^\circ$. Seven points were chosen at 20-mm intervals as test points as electric putter 1 changed from 440 mm to 320 mm. Corresponding values for θ_1 and p_{y1} were calculated from Eqs. (13) and (2), respectively; p_{y1} was negative because it changed in the negative *y* direction; θ_1 remained unchanged when $\theta_1=28.5^\circ$. Using six points at 10-mm intervals as test points as electric putter 2 changed from 225 mm to 275 mm, θ_3 and p_{y3} were calculated using Eqs. (14) and (2), respectively.

By analyzing the luffing process of the rear wheel-legged kinematics model (with actual installation angles of 10.28° and 25.4°),

$$\theta_{12}=\alpha-10.28^\circ+25.4^\circ \quad (15)$$

where α is the angle whose value changes with a change in the length of electric putter 4. For example, θ_{12} changed from 66° to 33.3° when the length of electric putter 4 changed from 470 mm to 350 mm. Using seven points at 20-mm intervals as test points as electric putter 4 changed from 470 mm to 350 mm, θ_{12} and p_{y12} (reference value relative to right-rear wheeled leg) were calculated using Eqs. (15) and (8), respectively; p_{y12} was negative because it changed in the negative *y* direction of the reference coordinate system; thus,

p_{y12}= -401*mm* (initial displacement relative to reference coordinate) and

$p_{y12\max}$= -241*mm* (final displacement relative to reference coordinates).

The maximal amplitude range of the right-rear wheeled leg in the *y* direction is

$$\left|p_{y12Y}\right| = \left|-401-(-241)\right| = 160mm$$

4. EXPERIMENTAL ANALYSIS

4.1. Simulation Experiment

Automatic Dynamic Analysis of Mechanical Systems (ADAMS) is a virtual prototype analysis software by Mechanical Dynamics Inc. that provides mechanical system simulations based on multi-body system dynamics theory. It can be used to create a fully parameterized dynamic model of a mechanical system using an interactive graphic environment, a parts library, a constraints base, and a mechanical library. This virtual platform provides three-dimensional (3-D) visualization of the system's motion in various simulation environments for design optimization. There are three basic modules for ADAMS: View, Solver, and Postprocessor. In this paper, the dynamics simulation of the obstacle-surmounting wheeled legs is based on the "View" module as showing in Fig. (**5**).

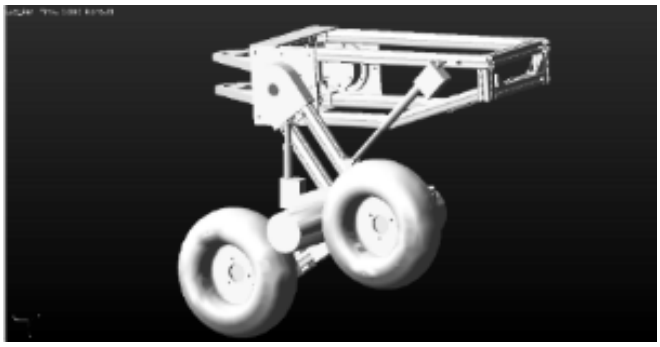

Fig. (5). Motion simulation of right-front wheeled leg.

The simulation data were derived, and the simulation curve of θ_1 and corresponding p_{y1} were obtained using Microsoft Excel, based on the mapping relationships because ADAMS provides only the relationship between p_y and time. In the same way, we obtained the simulation curves for θ_3 and p_{y3}, and θ_{12} and p_{y12}.

4.2. Test Method and Process

Test method: Classical proportional integral derivative (PID) control theory was adopted *via* CODESYS software to control the ESPC industrial controller. The motion displacements of electric putters 1 and 2 were measured precisely using angle and displacement sensors.

Test process: We used an electric putter with an L-linear motor (E05; speed: 10 mm s^{-1}) as shown in Fig. (**6**). The strokes of electric putters 1 and 2 were 120 mm and 50 mm, respectively. The stroke of electric putter 4 was 120 mm. For electric putters l, 2, and 4, the test points were the same as the points chosen for the theoretical calculation (Section 2.4). The test point numbers of electric putters l, 2, and 4 were 7, 6, and 7, respectively. The test points were measured three times to obtain an average value.

Fig. (6). Motion measurement graphic of the front wheel linear actuator 1.

5. ANALYSIS AND COMPARISON

After analyzing the kinetic characteristics of the wheel center 5 (in the right-front wheeled leg) as it encountered the luffing obstacle, we obtained measured and simulation curves for θ_1 and p_{y1}, θ_3 and p_{y3}, and θ_{12} and p_{y12}, as shown in Fig. (**7**).

6. DISCUSSION

1) In this study, the D-H method was adopted to establish a kinematics model of a six-wheeled luffing articulated chassis. According to the established kinematic model, a relationship between angle θ and p_y was obtained. The model was tested through simulations and experiments. The experimental results indicated a model accuracy of 98.3%. The front and rear wheeled legs demonstrated a vertical lift of 330.8 mm and 160 mm, respectively, which is sufficient for climbing applications in forested areas with stump heights of less than 100 mm [14-16].

2) Comparative analysis curves are shown in Fig. (**7**). The deviation between the simulation and theoretical curves was attributed to installation error and deformation of the chassis frame. For example, $\underline{p_{y1}}$ was smaller, due to the installation error that occurs when θ_1 ranges from 28.5° to 41.1°. Displacement deformation was the main influencing deviation factor when θ_1 was in the range of 41.1° to 51.3°.

3) Our analysis results showed that the maximum obstacle-surmounting height of the front wheeled legs and rear wheeled legs sufficiently met forestry production site conditions and forestry production demand for the chassis. The best barrier height was achieved by adjusting the position of the hinge points of triangles ΔAA_1A_2 and $\Delta B_1B_1B_2$.

CONCLUSION

A new type of six wheel-legged chassis for forestry production was designed. The D-H method was applied to establish a kinematics model of the chassis. Translation and rotation of the model's coordinate system allowed a positive motion attitude matrix to be obtained. The kinematics model

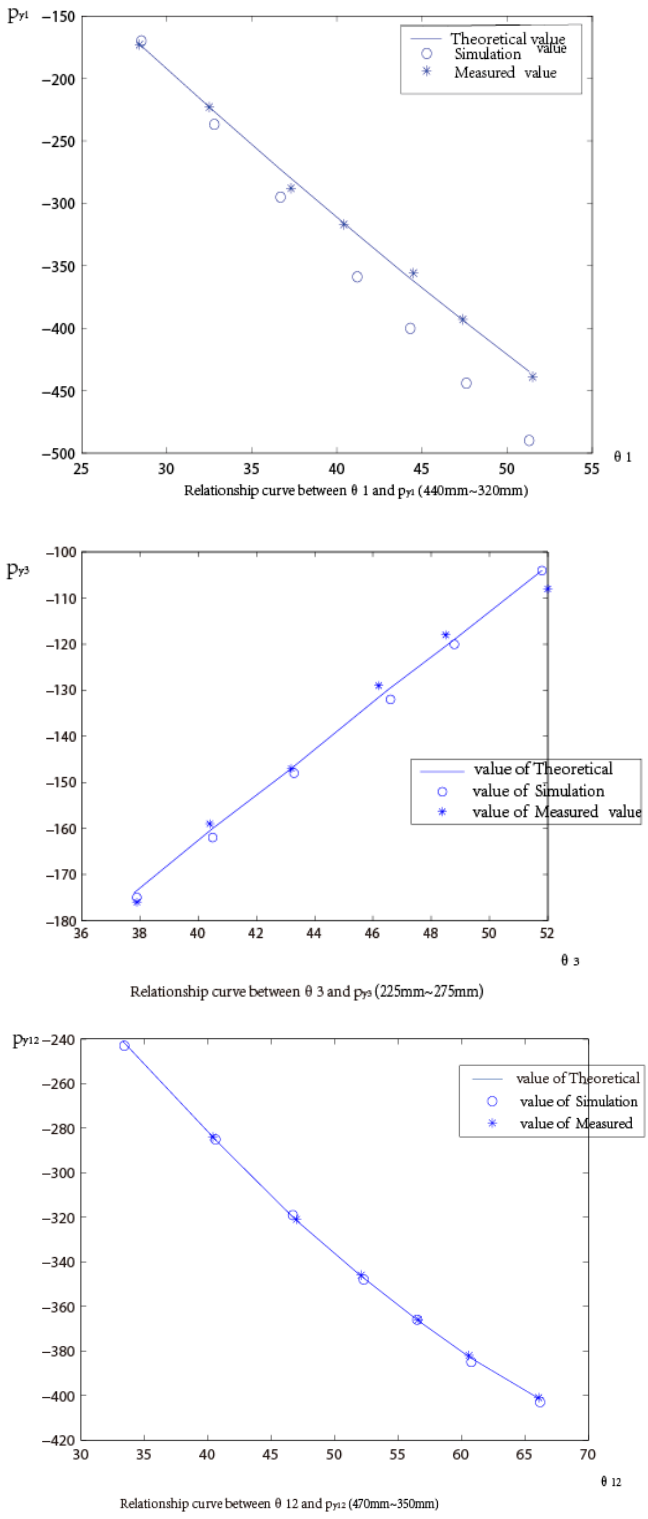

Fig. (7). Comparative analysis curves of p_{y1} *versus* θ_1, p_{y3} *versus* θ_3, and p_{y12} *versus* θ_{12}.

was calculated and analyzed, and tested against simulation and experimental data. Simulations and experimental results were in good agreement with the kinematic model and its positive solution. Our results are expected to guide future developments in forestry equipment and motion dynamic advances.

CONFLICT OF INTEREST

The authors confirm that this article content has no conflict of interest.

ACKNOWLEDGEMENTS

This work is supported by "the Fundamental Research Funds for the Central Universities TD2013-4". The authors would like to thank Dr. Huang Qingqing, Sun Zhibo, Li Cun for their important contribution to this work.

REFERENCES

[1] J. Xin, X. Li, Z. Wang, C. Yao, and P. Yuan, "Performance analysis of track-leg mobile robot in unstructured environment", *Robot*, vol. 26, pp. 35-39, 2004.

[2] K. Iagnemma, H. Shibly, A. Rzepniewski, and S. Dubowsky, "Planning and control algorithms for enhanced rough terrain rover mobility", In: *International Symposium on Artificial Intelligence, Robotics and Automation in Space*, Canadian Space Agency: Quebec, Canada, 2001, pp.1-8.

[3] A. Lamon Krebs, M. Lauria, R. Siegwart, S. Shooter, and P. Lamon, "Wheel torque control for a rough terrain rover", In: *IEEE International Conference on Robotics and Automation,* Piscataway, IEEE: NJ, USA, 2004, pp. 4682-4687.

[4] M. Hu, Z. Deng, H. Gao, and S. Wang, "Analysis of climbing obstacle trafficability on the six-wheeled rocker-bogie lunar rover". *Journal of Shanghai Jiaotong University*, vol. 39, pp. 928-932, 2005.

[5] Y. Gao, X. Wu, and Z. Wu, "Motion ability analysis and mechanism design for six-leg-wheel hybrid mobile robot", *Machinery Design & Manufacture*, vol. 6, pp. 171-176, 2003.

[6] Y. Xiong, *Robots,* Mechanical Industry Press: Beijing, 1993.

[7] Y. Chang, S. Ma, H. Wang, and D. Tan, "Method of kinematic modeling of wheeled mobile robot", *Journal of Mechanical Engineering*, vol. 46, pp. 30-35, 2010.

[8] M. Song, *Kinematics' Analysis of the Multi-Motion Mode Wheel-Leg Robot*, China: Hebei University of Technology, 2012.

[9] Z. Chen, and Q. Zhang, "The application of D-H method in the kinematics modeling of five-axis coordinated machine tools". *Machine Tool & Hydraulics*, vol. 35, pp. 88-90, 2007.

[10] H. Song, and H. Xu, "Kinematical analysis of the excavator working device based on D -H methodology", *Construction Machinery*, vol. 9, pp. 87-90, 2012.

[11] H. Ding, Y. Cao, Z. Yang, and L. Ma, "Position kinematics analysis of multi-linkage face-shovel excavator and envelope plotting using D-H method", *Journal of Yan Shan University*, vol. 38, pp. 198-203, 2014.

[12] M. Song, and M. Zhang, "Kinematics analysis for parallel mechanism of basic-mobile robot", *Journal of Agricultural Machinery*, vol. 43, pp. 200-206, 2012.

[13] Y. He, W. Liu, and C. Zhou, "Simulation of mutual motion between wheeled mobile robots and terrains", *Robots*, vol. 29, pp. 498-504, 2007.

[14] C. Meng, and F. Pang, "Research on Development of Stump", *Forest Engineering*, vol. 21, pp. 11-13, 2005.

[15] S. Xiao, "Research on suitable height of stump", *Journal of Northeast Forestry University*, vol. 27, pp. 42-45, 1999.

[16] C. Hong, R. Xue, and J. Han, "Confirmation of best cutting root height on the sprouting regeneration of Urophylla", *Forest Engineering*, vol. 19, pp. 11-12, 2003.

Received: February 17, 2014 Revised: March 21, 2015 Accepted: June 9, 2015